*DOI:*
10.1109/CIBCB.2019.8791475

*Document Version*
Peer reviewed version

# Development of a Deep Learning Method to Predict Optimal Ablation Patterns for Atrial Fibrillation


Marica Muffoletto*
*Department of Biomedical Engineering*
*King's College London*
London SE1 7EH, United Kingdom
marica.muffoletto@kcl.ac.uk

Xiao Fu
*Biomolecular Modelling Laboratory*
*The Francis Crick Institute*
London NW1 1AT, United Kingdom
xiao.fu@crick.ac.uk

Aditi Roy
*Department of Biomedical Engineering*
*King's College London*
London SE1 7EH, United Kingdom
aditi.roy@kcl.ac.uk

Marta Varela
*Department of Biomedical Engineering*
*King's College London*
London SE1 7EH, United Kingdom
marta.varela@kcl.ac.uk

Paul A. Bates*
*Biomolecular Modelling Laboratory*
*The Francis Crick Institute*
London NW1 1AT, United Kingdom
paul.bates@crick.ac.uk

Oleg V. Aslanidi
*Department of Biomedical Engineering*
*King's College London*
London SE1 7EH, United Kingdom
oleg.aslanidi@kcl.ac.uk



***Abstract*—Atrial fibrillation (AF) is a common cardiac arrhythmia that affects 1% of the population and is associated with high levels of morbidity and all-cause mortality. Catheter ablation (CA) has become one of the first line treatments for AF, but the success rates of CA and other clinical treatments remain suboptimal. The need to improve clinical outcomes warrants the optimisation of CA therapy. In this study, we develop a novel deep learning method to identify specific ablation patterns that terminate AF efficiently. To achieve this, we simulate typical AF ablation scenarios using computational models of 2D atrial tissue, and use the simulation outcomes as inputs for a deep neural network. The network is trained, validated and then applied to classify the scenarios and predict the optimal CA pattern in each scenario. For the validation dataset, the overall accuracy in identifying the best CA strategy is recorded at 79%. The study provides proof of concept that deep neural networks can learn from computational models of AF and help optimise CA therapy.**



***Index Terms*—atrial fibrillation, catheter ablation, tissue simulation, deep learning, therapy optimisation**


## I. Introduction

Atrial Fibrillation (AF) is the most common supraventricular arrhythmia and is characterised by rapid and uncoordinated contraction of the atria. It is associated with high levels of morbidity and is the number one cause of stroke in people over 75. [1] Although precise mechanisms underlying AF are still unclear, it has been recognised that ectopic electrical beats from the pulmonary veins (PV) can trigger AF [2], and that electrical rotors generated by breakdown of such ectopic waves provide self-sustained drivers for AF. In addition, areas of fibrotic atrial tissue have been linked with slow conduction of electrical waves, providing anchoring points for the rotors, and thus arrhythmogenic locations in the atria [3].

First line clinical treatments for AF include antiarrhythmic drugs, electrical cardioversion and catheter ablation therapy. Radiofrequency Catheter Ablation (RFCA) involves controlled destruction of arrhythmogenic locations via delivery of localised RF energy to atrial tissue through a catheter. RFCA procedures have relatively high success rate in patients with paroxysmal AF (about 70% for a single procedure) [4]. However, in persistent AF patients, the arrhythmia can recur after RFCA in ~75% of cases [5]. This warrants the development of novel, more efficient ablation strategies [6].

RFCA creates lines of conduction block on the atrial surface, which ideally should have minimal length and allow for quick recovery of the mechanical activity of both atria during sinus rhythm [7]. The only clinically proven empirical strategy is the Pulmonary Vein Isolation (PVI), which generates circumferential lesions around the right and left PVs. Promising novel strategies include rotor- and the fibrosis- driven CA. The former targets focal points of electrical activation to terminate rotors [8], while the latter aims to minimise the effect of fibrosis by applying box isolation of fibrotic areas (BIFA) [9] or linear lesions across fibrotic tissue [10].

The heterogeneous results obtained by different studies suggest that a single ablation strategy is unlikely to be successful for all patients, and the improvement of CA therapy can come from personalised approaches to each patient. We aim to simulate various scenarios of AF and personalised CA strategies using computational models on atrial tissue, and use the model simulation data to train deep neural networks, which have proven to be successful for time-series problems in biology [11], [12]. Once the network is built, we will use it to identify optimal patterns of CA lesions for each scenario.

## II. Methods

### A. Atrial tissue model

Propagation of electrical activation waves in cardiac tissue was simulated using the standard monodomain equation:

$$\frac{\partial V_m}{\partial t} = \nabla \cdot \mathbf{D} \nabla V_m - \frac{I_{ion}}{C_m} \tag{1}$$


Research supported by the British Heart Foundation (PG/15/8/31130).


*Corresponding author.

Here, $V_m$ represents the membrane voltage, $C_m$ is the specific cell capacitance, and **D** is the diffusion tensor that characterises electrical coupling in the tissue. For isotropic tissue the latter is a constant and it was set to 0.05 $mm^2ms^{-1}$.

Equation 1 was solved using forward Euler integration with a time step of 0.01 ms, combined with finite difference approximation of the Laplacian with a spatial step of 0.3 mm.

For simulation of the ion current, the Fenton-Karma semi-physiological model was used. This used three currents to model the main ionic currents responsible for the electrical activation and inactivation dynamics of atrial cells. These are the fast inward (flow of $Na^+$), the slow inward (flow of $Ca^{2+}$) and slow outward (flow of $K^+$) currents.

$$I_{ion} = I_{fi} + I_{so} + I_{si} \tag{2}$$

All the currents were described using the standard equations and parameters, as previously described [13], [14].

Equations 1 and 2 describe the propagation of electrical waves through atrial tissue. To generate the wave breakdown leading to rotors, the cross-field protocol was used [15]. To simulate different AF scenarios, each 2D tissue model was assigned 1) four circular areas of variable size and location corresponding to the PVs (with the diffusion coefficient and membrane potential both set to zero inside the area) and 2) a fibrotic patch of variable size and location (with $D = 0.0075$ $mm^2ms^{-1}$ to simulate slow conduction). Ablation lesions were simulated by setting values of the membrane potential and diffusion coefficient to zero in small circular areas corresponding to a catheter tip touching the tissue; zero-flux boundary conditions were applied around such areas, as well as the PVs.

Tips of the rotors - a focal point of its rotations - was tracked during the simulations. The tips were found as the intersection of isolines of $V_m$ and its time derivative [16]:

$$V(\mathbf{r}, n\Delta t) = V(\mathbf{r}, (n+1)\Delta t) = V_{iso} \tag{3}$$

The value of $V_{iso}$ used in the tracking was 0.8 mV.

### B. Data Collection

To train, test and validate our neural network classification algorithm (see section C below), our input datasets consisted of images from simulated electrical waves in 2D atrial tissue (section A), which corresponds to a 2D cross section of the upper left chamber of the heart, as shown in Fig. 1.

In total, 195 tissues were created with variable size and locations of the PVs and fibrotic patches, and respective AF scenarios were simulated in each tissue. The 2D tissues were labelled to represent common CA strategies: PVI, fibrosis-based and rotor-based ablation. Specifically, these were labelled according to success vs failure in 15 simulations for each of 195 tissues, each of 2000 ms duration. In 6 simulations fibrosis-based ablation was performed (2 for BIFA, 2 for nuclear ablation of the entire fibrotic areas and 2 for lesions across the fibrosis), then other 6 simulations PVI was performed (2 around a single vein, 2 around 2 pairs of veins, and 2 around all 4 veins), and in the last 3 simulations the tissue

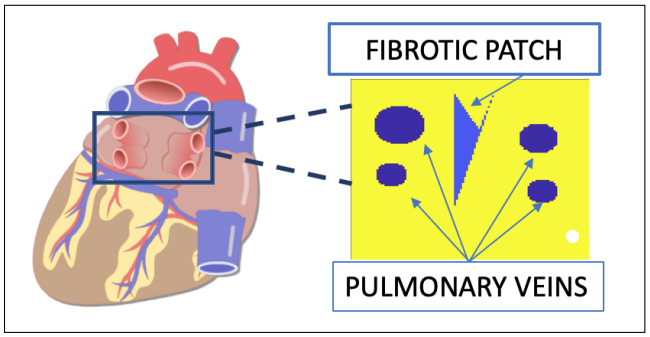


Fig. 1. Correspondence of 2D atrial tissue used in simulations with the 3D heart (posterior view). The 2D tissue corresponds to the left atrium projected on a plane, with the 4 pulmonary veins and a fibrotic patch present. This tissue geometry was used to simulate PVI and fibrosis-based ablation.

was ablated following the rotor tip trajectories. Since PVI is recognised as a standard successful treatment, simulations with no success over 2000 ms were also labelled as PVI.

Allocation of labels is described in Fig. 2. From this labelling method, we obtained a total of 73 tissues labelled as Rotor, 74 labelled as PVI, and 48 labelled as Fibrosis. The total number of 195 tissue images used as input for the network was further subdivided into 156 images for training, 39 for validation and 20 for testing.

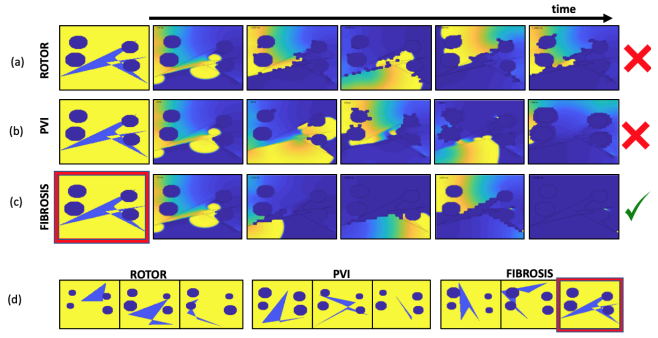


Fig. 2. Simulations and label assignment for each 2D tissue. Before assigning the label, the rotor-based CA strategy shown in part (a) was simulated 3 times; the PVI (b) and fibrosis-based (c) strategies were each simulated 6 times. The label was assigned based on the maximum number of successful AF terminations across all the trials. Horizontal arrow shows the time axis and five panels under it are the voltage distributions in 2D tissue for successive moments of time. Green tick and red cross indicate CA success and failure, respectively. In the example shown, the tissue shown on the right (red frame) was assigned Fibrosis label. Part (d) shows several examples of labelled tissues derived from this process, which represent a subset of the training data.

### C. Convolutional Neural Network

To identify optimal CA patterns, a classification algorithm was applied to the tissues. This was constructed using Tensor Flow [17], in conjunction with the Python Keras library [18].

Pre-processing of the data consisted in resizing of the image to a standard size of 64x64 pixels and normalization.

The Convolutional Neural Network (CNN) architecture consisted of two 2D convolutions made of 32 filters, each of size 3x3, followed by Rectified Linear Unit (ReLU) activation and using maxnorm constraint. The convolution block was

followed by a MaxPooling with pool size 2x2, a Flatten layer, and two Dense layers, the first of which was made of 512 units and had ReLU activation and maxnorm kernel constraint. This was followed by a Dropout layer of rate 0.5. The second Dense Layer used softmax activation.

The optimizer chosen was a stochastic gradient descent (sgd) with a learning rate of 0.01. The number of epochs was set to 300. The algorithm was also tested for epoch values of 2000 and 5000, but no increase in accuracy was observed.

## III. Results

The value for the total accuracy in predicting the optimal CA strategy reported by the algorithm for 39 validation images is 79.49%. The results are validated against CA success vs failure seen in the respective simulations. Precision, Recall and f1-score were calculated for each class, and these are summarised in Table I. Precision seems to be relatively high for PVI and Rotor classes, while decreasing to 50% for Fibrosis; this can be due to the lower data available for this class. Recall value for Fibrosis is not affected by this, therefore overall the algorithm shows good sensitivity. The F1-score is an harmonic mean of the previous two values; it shows a really high performance of the Rotor class, giving an overall inter-class gap of 27%.

TABLE I
Evaluation of Network through classes

| | precision | recall | f1-score |
|---|---|---|---|
| Fibrosis | 0.50 | 0.88 | 0.64 |
| Pvi | 1.0 | 0.70 | 0.82 |
| Rotor | 0.91 | 0.91 | 0.91 |
| micro avg | 0.79 | 0.79 | 0.79 |
| macro avg | 0.80 | 0.83 | 0.79 |
| weighted avg | 0.87 | 0.79 | 0.81 |

Fig. 3 shows the change in accuracy for the training and test data over 300 epochs. When tested over the validation data, the algorithm shows a high performance and stability (within epoch 40 an accuracy of 0.86 is obtained).

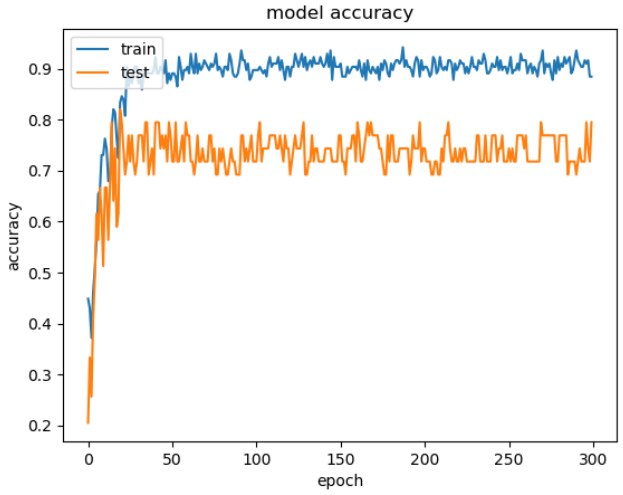


Fig. 3. Classification accuracy over 300 epochs for training and test data.

When using the test data, it can be seen (Fig. 3) that longer training doesn't improve the accuracy significantly. In fact, the maximum value is reached just before epoch 30, and then it stabilises in the range of 0.7-0.8. A possible solution to smooth this curve and increase the accuracy in the training set could be to apply an adaptive learning rate; we also expect that increasing the amount of training data would result in a better performance of the classification algorithm.

Table II summarises results for predicted labels (CA strategies) for the test set of 20 tissues. Some of the prediction probabilities are very high, confirming the obtained precision and recall seen in Table I.

TABLE II
Algorithm predictions on test data

| test | prediction | probability | test | prediction | probability |
|---|---|---|---|---|---|
| 1 | Rotor | 0.99 | 11 | Fibrosis | 1 |
| 2 | Rotor | 0.54 | 12 | Fibrosis | 0.99 |
| 3 | Rotor | 0.99 | 13 | Fibrosis | 1 |
| 4 | PVI | 1 | 14 | PVI | 1 |
| 5 | Rotor | 0.55 | 15 | Fibrosis | 1 |
| 6 | Rotor | 1 | 16 | Rotor | 1 |
| 7 | Fibrosis | 0.99 | 17 | Rotor | 1 |
| 8 | PVI | 0.8 | 18 | Rotor | 0.54 |
| 9 | Rotor | 0.68 | 19 | Rotor | 0.99 |
| 10 | PVI | 0.99 | 20 | PVI | 1 |

All the labels predicted by the algorithm were confirmed by the simulations, except from two test samples, number 2 and 8. Test number 2 is a tissue resulting in a very low percentage of success over all the simulations, where only 1 PVI strategy succeeded. The same can be said for test number 8 where only 1 rotor strategy had a positive result. It is certainly less straightforward for the algorithm to predict a suitable CA therapy of a specific tissue for which simulations also produce a poor outcome. Ultimately, this issue can be fixed by increasing the number of simulations for each tissue in order to provide more accurate labels to each image.

It is worth noting that we would have expected to see more Fibrosis labels misplaced but instead the tested subset gave optimal predicted values for this class.

## IV. Conclusion

This work has demonstrated proof of concept: deep neural networks can be constructed to learn from computational simulations of atrial electrical activations, to identify optimal locations to administer ablations, thereby treating AF. Moreover, the method constructed enabled us to predict optimal CA patterns for new tissues, with randomly assigned fibrotic patch locations and topologies, which is currently one of the ultimate aims of research in the field of AF. The results in Table II show accurate predictions on a small subset of new data, and therefore, provide confidence for the utility of further algorithm development.

The main limitation of the current approach is the absence of sufficient data for training. Moreover, a detailed analysis should be conducted on interesting cases where PVI, Rotor

and Fibrosis patterns give the same rate of success for a tissue, which here have all been labelled as PVI. A more effective way to deal with these situations is to compare the percentage of tissue ablated for each pattern, which for the simulations carried out in this study never exceeded 42% of tissue ablated.

Successive steps would be to further tune the hyperparameters used for the classification algorithm and to increase the number of training data. Ultimately, our aim would be to apply a similar research study to 3D data gathered through simulations of real patient MRI scans, as suggested by Fig. 4.

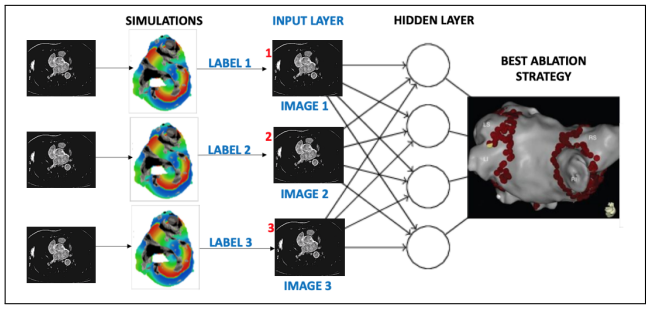


Fig. 4. Proposed workflow for assigning labels to patient MR images based on image-derived 3D simulations of atrial electrical activations. Similar to the current study, labels would be given to each patient datasets according to the rate of success for several AF ablation scenarios. Once passed through the layers of a CNN, the output would be the best CA strategy for a given patient.

Despite of the current data volume limitations, this work allowed us to highlight the importance of a patient-specific approach to AF therapy, which is being increasingly recognised [19]–[21]. Moreover, we identified CNNs as a new tool to investigate different patterns for optimal CA therapy. The results obtained show that a neural network can provide a sensible approach to identify a suitable ablation strategy for the considerably high number of people suffering from AF. Specifically, it would be of significant importance if applied on a detailed 3D image-based model that includes atrial geometry and fibrosis [3], [14], as well as other MRI-derived structural features such as the atrial wall thickness [22].

## REFERENCES


[1] R. G. Hart and J. L. Halperin, "Atrial fibrillation and stroke : concepts and controversies." *Stroke*, vol. 32, no. 3, pp. 803–8, 2001.

[2] S. A. Chen, M. H. Hsieh, C. T. Tai, C. F. Tsai, Prakash *et al.*, "Initiation of atrial fibrillation by ectopic beats originating from the pulmonary veins: Electrophysiological characteristics, pharmacological responses, and effects of radiofrequency ablation," *Circulation*, vol. 100, no. 18, pp. 1879–1886, 1999.

[3] R. Morgan, M. Colman, H. Chubb, G. Seemann, and O. Aslanidi, "Slow conduction in the border zones of patchy fibrosis stabilizes the drivers for atrial fibrillation: Insights from multi-scale human atrial modeling," *Frontiers in Physiology*, vol. 7, no. 474, 2016.

[4] N. Oketani, H. Ichiki, Y. Iriki, H. Okui, M. Ryuichi, N. Fuminori, Y. Ninomiya, S. Ishida, S. Hamasaki, and C. Tei, "Catheter ablation of atrial fibrillation guided by complex fractionated atrial electrogram mapping with or without pulmonary vein isolation," *Journal of Arrhythmia*, vol. 28, no. 6, pp. 311 – 323, 2012.

[5] Y. Wang, Y. Xu, Z. Ling, W. Chen, L. Su, H. Du, P. Xiao, Z. Liu, and Y. Yin, "Radiofrequency catheter ablation for paroxysmal atrial fibrillation: over 3-year follow-up outcome," *Journal of the American College of Cardiology*, vol. 70, no. 16 Supplement, p. C126, 2017.

[6] Y. Gong, Y. Gao, Z. Lu, D. Zheng, D. Deng, and L. Xia, "Preliminary simulation study of atrial fibrillation treatment procedure based on a detailed human atrial model," *Journal of Clinical Trials in Cardiology*, vol. 2, pp. 01–09, 2015.

[7] P. Ruchat, L. Dang, N. Virag, J. Schlaepfer, L. K. von Segesser, and L. Kappenberger, "A biophysical model of atrial fibrillation to define the appropriate ablation pattern in modified maze," *European Journal of Cardio-thoracic Surgery*, vol. 31, no. 1, pp. 65–69, 2007.

[8] J. A. Zaman, N. S. Peters, and S. M. Narayan, "Rotor mapping and ablation to treat atrial fibrillation," *Current Opinion in Cardiology*, vol. 30, no. 1, pp. 24–32, 2015.

[9] D. Schreiber, A. Rieger, F. Moser, and H. Kottkamp, "Catheter ablation of atrial fibrillation with box isolation of fibrotic areas: Lessons on fibrosis distribution and extent, clinical characteristics, and their impact on long-term outcome," *Journal of Cardiovascular Electrophysiology*, vol. 28, no. 9, pp. 971–983, 2017.

[10] "Therapeutic Approaches to Atrial Fibrillation Ablation Targeting Atrial Fibrosis," *JACC: Clinical Electrophysiology*, no. 7, pp. 643–653, 2017.

[11] Y. Wu, M. Schuster, Z. Chen, Q. V. Le, M. Norouzi *et al.*, "Google's neural machine translation system: Bridging the gap between human and machine translation," *ArXiv*, pp. 1–23, 2016.

[12] E. Pfeiffenberger and P. A. Bates, "Predicting improved protein conformations with a temporal deep recurrent neural network," *PLoS One*, vol. 13, no. 9, 2018.

[13] A. Peñaranda, I. R. Cantalapiedra, J. Bragard, and B. Echebarria, "Cardiac dynamics: A simplified model for action potential propagation," *Theoretical Biology and Medical Modelling*, vol. 9, no. 1, pp. 1–18, 2012.

[14] "Image-based computational evaluation of the effects of atrial wall thickness and fibrosis on re-entrant drivers for atrial fibrillation," *Frontiers in Physiology*, vol. 9, no. 1352, pp. 1–16, 2018.

[15] C. Tobón, L. Palacio, J. Duque, E. Cardona, J. Ugarte, A. Orozco-Duque, M. Becerra, J. Saiz, and J. Bustamante, "Simple ablation guided by apen mapping in a 2d model during permanent atrial fibrillation," *Computing in Cardiology*, vol. 41, pp. 1029–1032, 2014.

[16] F. Fenton and A. Karma, "Vortex dynamics in three-dimensional continuous myocardium with fiber rotation: Filament instability and fibrillation," *Chaos (Woodbury, N.Y.)*, vol. 8, pp. 20–47, 1998.

[17] M. Abadi, P. Barham, J. Chen, Z. Chen, A. Davis *et al.*, "Proceedings of the 12th usenix conference on operating systems design and implementation," pp. 265–283, 2016.

[18] K. Chauhan and S. Ram, "Image classification with deep learning and comparison between different convolutional neural network structures using tensorflow and keras," *International Journal of Advance Engineering and Research Development*, vol. 2, no. 02, 2018.

[19] N. Soor, R. Morgan, M. Varela, and O. V. Aslanidi, "Towards patient-specific modelling of lesion formation during radiofrequency catheter ablation for atrial fibrillation," *2016 38th Annual International Conference of the IEEE Engineering in Medicine and Biology Society (EMBC)*, pp. 489–492, 2016.

[20] C. H. Roney, I. Sim, J. Whitaker, L. ONeill, M. ONeill, O. Razeghi, R. K. Mukherjee, S. E. Williams, S. A. Niederer, H. Cochet, E. J. Vigmond, and G. J. Klein, "Patient-specific simulations predict efficacy of ablation of interatrial connections for treatment of persistent atrial fibrillation," *EP Europace*, vol. 20, no. suppl_3, pp. iii55–ii68, 2018.

[21] H. Cochet, R. Dubois, S. Yamashita, N. Al Jefairi, B. Berte, Sellal *et al.*, "Relationship between fibrosis detected on late gadolinium-enhanced cardiac magnetic resonance and re-entrant activity assessed with electrocardiographic imaging in human persistent atrial fibrillation," *JACC: Clinical Electrophysiology*, vol. 4, no. 1, pp. 17–29, 2018.

[22] M. Varela, R. Morgan, A. Theron, D. Dillon-Murphy, H. Chubb, J. Whitaker, M. Henningsson, P. Aljabar, T. Schaeffter, C. Kolbitsch, and O. V. Aslanidi, "Novel mri technique enables non-invasive measurement of atrial wall thickness," *IEEE Transactions on Medical Imaging*, vol. 26, pp. 1607–1614, 2017.